ROYAL SOCIETY OF CHEMISTRY

PAPER

Check for updates

Coordination mechanism of cyanine dyes on the surface of core@active shell β-NaGdF₄:Yb³⁺,Er³⁺ nanocrystals and its role in enhancing upconversion luminescence†

Hossein Beygi Nasrabadi, [ID] [a] Eduard Madirov, [b] Radian Popescu, [c] Lenka Štacková, [d] Peter Štacko, [ID] [d] Petr Klán, [ID] [d] Bryce S. Richards, [ID] *[ae] Damien Hudry[a] and Andrey Turshatov [ID] *[a]

The sensitization of lanthanide-doped upconversion nanocrystals (UCNCs) using organic dyes with a broad and intense optical absorption is an interesting approach for efficient excitation-energy harvesting and enhancing the upconversion luminescence of such UCNCs. In this work, an ultrasmall (~6.5 nm in diameter) β-NaGdF₄:Yb³⁺,Er³⁺ core and related core@shell UCNCs were sensitized using six NIR-excitable cyanine dyes with a wide range of functional groups and optical properties. The greatest UC enhancement of 680-times was observed for the conjugate between the Cy 754 dye and NaGdF₄:Yb³⁺,Er³⁺@NaGdF₄:10%Yb³⁺,30%Nd³⁺ core@shell UCNCs excited using a 754 nm laser. The enhancement was estimated relative to NaGdF4:Yb³⁺,Er³⁺@NaGdF₄:10%Yb³⁺,30%Nd³⁺ core@shell UCNCs capped with oleic acid and excited using a similar intensity (75 W cm⁻²) of a 980 nm laser. UC intensity measurements for identical dye-sensitized UCNCs carried out in methanol and in deuterated methanol under argon, as well as in air, allowed us to reveal the connection of the dye triplet states with UCNC sensitization as well as of the hydroxyl groups with quenching of the excited states of lanthanide ions. For UCNCs dispersed in methanol, the strong quenching UC luminescence was always observed, including core@shell UCNCs (with a shell of ~2 nm). A strong influence of the triplet states of the dyes was observed for the two dyes Cy 754 and Cy 792 that bind firmly to UCNCs and allow the distances between the dye and the UCNC to be reduced, whereas the contribution of this sensitization pathway is very insignificant for Cy 740 and Cy 784 dyes that bind weakly to UCNCs.

Introduction

Upconversion nanocrystals (UCNCs) constitute an optically inert crystalline host material doped with trivalent lanthanide (Ln³⁺) ions to realize optical functionality.[1] Taking advantage of

[a] *Institute of Microstructure Technology (IMT), Karlsruhe Institute of Technology, Hermann-von-Helmholtz-Platz 1, Eggenstein-Leopoldshafen, 76344, Germany. E-mail: bryce.richards@kit.edu, andrey.turshatov@kit.edu*

[b] *Kazan Federal University, Institute of Physics, 18 Kremlevskaja str., Kazan, 420008, Russia*

[c] *Laboratory of Electron Microscopy, Karlsruhe Institute of Technology, Engesserstrasse 7, D-76131 Karlsruhe, Germany*

[d] *Department of Chemistry and RECETOX, Masaryk University, Kamenice 5, 625 00 Brno, Czech Republic*

[e] *Light Technology Institute (LTI), Karlsruhe Institute of Technology, Engesserstrasse 13, 76131 Karlsruhe, Germany*

† Electronic supplementary information (ESI) available: Detailed experimental and characterization methods, NMR and FITR spectra, supplementary TEM and XRD graphs, luminescence and UC luminescent transients, and transient absorption spectra. See DOI: 10.1039/d1tc03333f

the ladder-like hierarchy of long-lived intermediate energy states within the Ln³⁺ ions, UCNCs can sequentially absorb several long-wavelength photons and convert them into shorter-wavelength radiation,[1–3] with Er³⁺ being the most commonly studied species. Because of their high photochemical stability, narrow emission bandwidth, long luminescence lifetimes, and large anti-Stokes shift, UCNCs have attracted broad interest in many research areas, including biological imaging, drug delivery, photodynamic therapy, volumetric displays, and solar cells.[1–6] Despite these promising advantages, low upconversion quantum yields (ϕ_{UC}) and brightness of the upconverted emission (B_{UC}) – defined as the product of the molar absorption coefficient (at the relevant excitation wavelength) and the fluorescence quantum yield ($\phi_{UC} \times \varepsilon_\lambda$)[7] – mean that UCNCs have been limited in their practical applications.[3,8] Although efforts have been made to enhance the B_{UC} and ϕ_{UC} of UCNCs – such as coating UCNCs with inert or active shells,[9] optimizing the type and the concentration of lanthanide ions,[10] and surface–plasmon coupling[11] – the low photon-harvesting

This journal is © The Royal Society of Chemistry 2021

J. Mater. Chem. C, 2021, **9**, 16313–16323 | **16313**

efficiency of UCNCs remains a challenge. This fundamental limit is mainly associated with the parity-forbidden nature of the 4f–4f electronic transitions of the Ln^{3+} ions, which causes the sensitizer ions to absorb light in a narrow spectral window and with a critically small absorption cross-section.[3,8]

In 2012, the Hummelen group[12] proposed a dye-sensitization strategy to address this performance-limiting problem, yielding up to 3300-fold B_{UC} enhancement of UCNCs. *Via* this route, organic dye molecules with a spectrally broad and intense absorption were coupled to UCNCs. The dyes function as antennae, harvesting the excitation light energy and transferring them *via* Förster resonance energy transfer (FRET) to the Ln^{3+} ions incorporated in the UCNCs. Compared to commonly used Yb^{3+} sensitizers, organic dyes have a much higher optical absorption owing to their ∼10 times wider absorption band and their ∼5 × 10⁶ times higher molar absorption coefficient. Moreover, the broad absorption width of organic near-infrared (NIR) dyes makes it possible to flexibly tune the excitation wavelengths of UCNCs.[12–14] These advantages can be applied in areas such as photovoltaics and photocatalysis,[15] bio-sciences[16] and anti-counterfeiting technologies.[17]

In recent years, a variety of organic dye molecules with broad absorption spectra and high absorption cross-sections have been evaluated for sensitizing UCNCs.[14,18–20] The main objective of such studies is the enhancement of the energy-transfer efficiency from the dye to the UCNCs due to a better spectral match between dye luminescence and the absorption spectra of Ln^{3+} sensitizers. Therefore, most of the dye molecules exhibit a strong absorption over a wide range of visible and NIR wavelengths (∼500–950 nm). The emission bands of these dye molecules in the NIR range (750–1100 nm) overlap with the absorption spectrum of Yb^{3+} (at ∼980 nm) and Nd^{3+} (at 740 and 808 nm). For example, indocyanine green (ICG) dye possesses a broad absorption spectrum between 680 and 880 nm. Its absorption cross-section (∼6 × 10⁻¹⁶ cm²) is around 30 000-times higher than that of Nd^{3+} ions (∼2 × 10⁻²⁰ cm²) at 808 nm, and thus efficient photosensitization of UCNCs is expected.[21] Moreover, the dye molecules with absorption bands in the visible wavelength range can be utilized for sensitizing other luminescent Ln^{3+} ions such as Tb^{3+} and Eu^{3+}, as well as for designing upconversion luminescence resonance energy transfer (LRET) sensors,[22–25] and down-conversion NCs.[26–28]

Although coating the UCNCs with a protective un-doped shell has been recognized as a robust strategy for minimizing the surface quenching of the lanthanide ions and enhancing the B_{UC} and ϕ_{UC}, the inert shell has an adverse effect on the dye-sensitized UC emission since it blocks energy transfer from the dye to the UCNCs.[23,29] To overcome this drawback, coating the UCNCs with an active shell doped with Yb^{3+} has been reported to increase the UC luminescence by a factor of 8–20 compared with the dye-sensitized UCNCs alone.[23,30,31] In addition, further B_{UC} enhancement of dye-sensitized UCNCs could be achieved by doping Nd^{3+} into the active shell layer.[9] Here, Nd^{3+} shifts the absorption peak of the UCNCs from that of Yb^{3+} at 980 nm to the wavelength of Nd^{3+} peak at 808 nm, which is more favorable for bioimaging excitation.[32]

In addition, the absorption cross-section of Nd^{3+} is ∼10 times higher than that of Yb^{3+}, so Nd^{3+} incorporation into the shell layer can markedly boost the capture ability of excitation photons.[33] Furthermore, it has been reported that doping both the Nd^{3+} and Yb^{3+} sensitizers into the shell layer provides a highly effective transfer of the harvested energy from the dye molecules to the Ln^{3+} ions in the core of the UCNCs.[29,34]

A recent study by Garfield *et al.*[35] discovered a critical role of triplet states of dye antennas in the B_{UC} and the stability of dye-sensitized UCNCs. It was demonstrated that the time-gated luminescence spectrum of the IR 806 dye exhibits only a weak spectral overlap of the dye singlet state with Yb^{3+} absorption, whereas the triplet state in the dye antennas (with the strong spectral overlap) acts as the key intermediate in the sensitization of the UCNCs. On this point, heavy lanthanide ions – for instance, Gd^{3+} in $NaY_xGd_{(1−x)}F_4$ UCNCs – can enhance inter-system crossing (ISC) in the adsorbed dye and triplet state population and, thus, increase B_{UC} when compared with the lighter element $NaYF_4$-based host.[35]

Despite recent progress in the design and efficiency enhancement of dye-sensitized UCNCs, several basics governing the foundation of such structures require further experimental investigations. First, the attachment mechanism of the dye molecules to the surface of the UCNCs, their binding stability, the distance between the dye and the UCNCs, and the equilibrium number of dyes per particle need to be better understood. Second, the effects of surface impurities (unbound dyes, remaining oleate, small ionic species appearing after a ligand-exchange process such as the OH groups, hydroxyl anions OH^- or BF_4^-) on the B_{UC} and ϕ_{UC} values of such hybrid nanostructures deserves more attention. Third, the proposed mechanism of energy transfer from the triplet states of the dye to the Ln^{3+} ions in the UCNCs requires a special study. This mechanism was not confirmed recently by Liu *et al.* for CaF_2:30%Yb^{3+} and CaF_2:30%Yb^{3+}@CaF_2:30%Ln^{3+} (Ln^{3+}–Nd^{3+} or Gd^{3+}) UCNCs.[36] The results of transient absorption spectroscopy, steady-state photoluminescence (PL) measurements, and PL decay curves indicated that the energy transfer from fluorescein isothiocyanate (FITC) and IR806 dyes to Ln^{3+} ions was dominated by the excited singlet state with no evidence of excited dye triplets. In this respect, it is not completely clear what advantages triplet states can offer for enhancing the B_{UC} and ϕ_{UC} in the case of dye-sensitized core@shell UCNCs. Finally, it is also not obvious whether or not sensitization of the dye is beneficial for solar energy harvesting applications – like photovoltaics and photocatalysis – as a direct comparison of the best dye-sensitized UCNCs and optimized core@shell UCNCs has not yet been performed.

In this research, novel cyanine dyes were synthesized to exhibit a wide range of absorption/emission bands, specifically for sensitizing UCNCs. A range of cyanine dyes with different functional groups was chosen to investigate the dye-attachment mechanisms, and to evaluate the equilibrium dye : UCNCs ratios. It was assumed that, due to steric and electrostatic restrictions, full coverage of the UCNC surface with the dye molecules does not occur, so hydroxylation of an unpassivated part of the UCNC surface can be a reason for triplet and luminescence quenching. To examine the energy transfer from

16314 | *J. Mater. Chem. C*, 2021, **9**, 16313–16323

This journal is © The Royal Society of Chemistry 2021

the triplet state of the dyes to the UCNCs, some approaches are employed to enhance the ISC via: (i) designing the dye molecules with heavy iodine atoms;[37] (ii) synthesizing UCNCs with an optimized heavy atom concentration based on the previous report by Garfield et al.;[35] and (iii) sensitization of the dye in an OH/O$_2$-free environment. Furthermore, this paper answers the question of whether or not the design of a shell layer around the UCNCs can prevent luminescence quenching and simultaneously allow singlet/triplet energy transfer from the dye molecules to the Ln^{3+} ions of the UCNCs. The newly-found fundamental insights regarding the design of efficient dye-sensitized UCNCs are demonstrated with dye and small core@-shell UCNCs (10 nm) resulting in a 680-fold B_{UC} enhancement.

Results and discussion

Synthesis of NaGdF$_4$:Yb^{3+},Er^{3+} UCNCs and optical properties of the cyanine dyes

Ultrasmall NaGd$_{0.8}$F$_4$:Yb$_{0.18}$,Er$_{0.02}$ UCNCs with an average size of ~6.5 nm were synthesized using the method reported by Wang et al.,[38] with some modifications as detailed in ref. 39. According to the transmission electron microscopy (TEM) images and the size distribution histogram in Fig. 1A, the as-synthesized UCNCs exhibit a spherical morphology and are highly monodisperse. The X-ray diffraction (XRD) pattern in Fig. 1B suggests that the synthesized UCNCs have the hexagonal β-NaGdF$_4$:Yb,Er phase structure (in perfect agreement with JCPDS-No. 27-0699), with no indication of the cubic α-phase

formation. Given their ultrasmall particle size and their high surface-to-volume ratio, it is not surprising that the synthesized UCNCs exhibit a high rate of luminescence quenching and, subsequently, a low UC efficiency. Thus, dye-sensitization offers the possibility of a significant brightness enhancement in such UCNCs. It should also be noted that all NaGdF$_4$:Yb^{3+},Er^{3+} UCNCs utilized for the dye-sensitizing processes were synthesized in a single batch, which makes it possible to compare the effects of different dye-sensitization processes for exactly the same type and concentration of UCNCs.

To investigate the effect of the dye structure on its attachment to the UCNC and any subsequent enhancement of the UC luminescence, six types of cyanine dyes were synthesized according to the methods described in the literature[37,40] (Table S1, ESI†). The chemical structures of the synthesized cyanine dyes are shown in Fig. 1C, with attachment on the surface of the UCNCs being possible via their carboxylic or sulfonate groups.

Here, the synthesized dyes are labeled as Cy 740, Cy 748, Cy 754, Cy 778, Cy 784, and Cy 792 based on their absorption peaks in methanol (MeOH) solutions at 740, 748, 754, 778, 784, and 792 nm, respectively (as illustrated in Fig. 1D). The dyes exhibit Stokes shifts of 34, 39, 40, 88, 46, and 45 nm, respectively, with the fluorescence spectra peaking between 774 and 866 nm (Fig. 1E). The chemical composition characteristics and photophysical properties of the synthetic cyanine dyes are given in Table S1 (ESI†). Furthermore, Fig. S1–S9 (ESI†) show the nuclear magnetic resonance (NMR) and Fourier-transform infrared (FTIR) spectroscopy patterns of the synthetic cyanine dyes, confirming the successful synthesis of the designed dyes.

Fig. 1 (A) Transmission electron microscopy (TEM) images and size-distribution histogram indicate the synthesis of monodisperse β-NaGdF$_4$:Yb,Er UCNCs with an average diameter of ~6.5 nm. (B) X-ray diffraction (XRD) pattern (red line) of the UCNCs perfectly matched the β-NaGdF$_4$:Yb,Er pattern (JCPDS-No. 27-0699). (C) Molecular structures of the cyanine dyes, along with (D) the normalized absorption spectra of the cyanine dyes in MeOH and (E) the normalized emission spectra of the synthetic cyanine dyes in MeOH under 740 nm laser excitation.

This journal is © The Royal Society of Chemistry 2021

J. Mater. Chem. C, 2021, **9**, 16313–16323 | **16315**

Surface modification of NaGdF$_4$:Yb,Er UCNCs with the cyanine dyes

The first step in dye-sensitization of the β-NaGdF$_4$:Yb^{3+},Er^{3+} UCNCs was an HCl treatment process applied to oleic acid (OA)-capped UCNCs for removing all oleate ligands. In the HCl treatment we followed the protocol described by Bogdan et al.[41] with some modifications (see the ESI† section). It has been repeatedly reported that this process effectively removes OA, while preserving the size and structure of the UCNCs.[42,43] After HCl treatment, the ligand-free UCNCs can be dispersed in polar solvents like MeOH along with the cyanine dyes, where the dyes have a high tendency to attach to the surfaces of the UCNCs. To investigate the dye–UCNC attachment mechanism and the ratio of dye molecules to UCNCs, all the experiments were conducted using a similar concentration of dyes and UCNCs. Detailed experimental information on the dye sensitization conditions is given in the ESI.† In these experiments, excess dye concentrations of 3 μg ml^{-1} were chosen so that some free dye molecules are still present in the solutions. The MeOH solutions were subsequently purified by centrifugation processes to remove such free dyes. Here, the supernatant phase consists of free dyes, while the precipitate contains the UCNCs with the bonded dyes and some remaining free dyes. By dispersion of the precipitate in fresh MeOH and repeating the centrifugation process, the free dyes can be completely separated from the surfaces of UCNCs after several purification cycles. The absorption spectra of MeOH solutions before each purification step and also the absorption spectra of the supernatant solutions after each purification step were measured under the same conditions (Fig. S7–S12, ESI†). While both bound and free dyes participate in the absorption spectra of MeOH solutions before purification, only the free dyes are responsible for the absorption spectra of the supernatant after the centrifugation process. Therefore, the difference in the absorption spectra of MeOH solutions before and after the purification step is a measure of the concentration of bound dyes and, subsequently, the number of bound dyes per UCNC.

Fig. 2 displays the variation in the absorption of the MeOH solutions before and after each purification step for the six dyes. In general, three trends of absorption peak variations are observed, suggesting three different mechanisms of dye–NC attachment:

(i) In the case of UCNCs sensitized with Cy 754 and Cy 792 dyes (Fig. 2A and B), the absorption intensity of the supernatant solution is zero after three purification steps, suggesting the complete removal of free dyes from the supernatant solution. Likewise, the concentration of attached dyes on the surface of UCNCs becomes constant after three purification steps, meaning that the dyes are firmly bound to the particle surface, and the prepared colloids contain just the bonded dyes. According to the concentration of dyes and UCNCs in the solutions, ∼17 molecules of Cy 754 and ∼15 molecules of the Cy 792 dye are attached to the surface of each UCNC (details of the calculation method are given in Section S7, ESI†). Regarding the molecular structures and functional groups of such dyes (Fig. 1C), the Cy 792 and Cy 754 dyes appear to be firmly bound to the particle surface due to the strong coordination of the carboxylic and sulfo groups with the ion centers
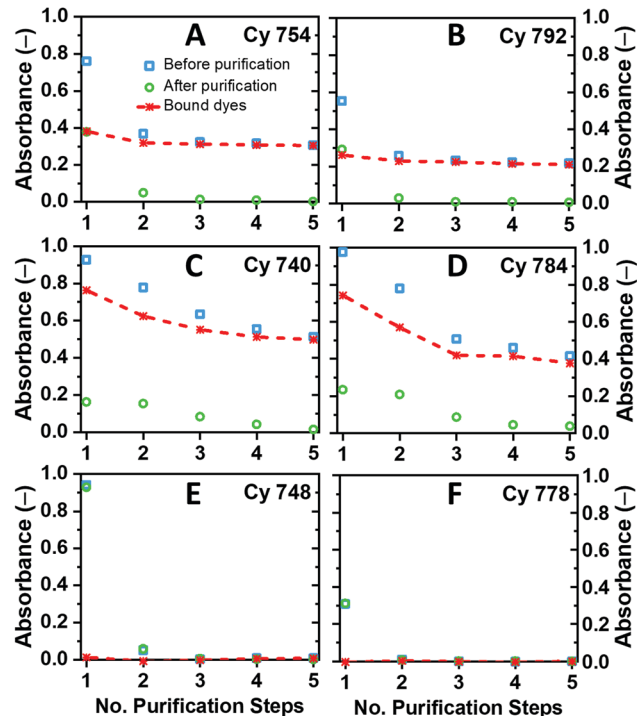

Fig. 2 Absorption peak intensity variations for MeOH solutions of NaGdF$_4$:Yb,Er UCNCs with Cy 754 (A), Cy 792 (B), Cy 740 (C), Cy 784 (D), Cy 748 (E), and Cy 778 (F) dyes. The initial dye concentrations are similar in all the experiments (3 μg ml^{-1}). The blue square symbols show the absorption intensities of MeOH solutions before each purification step, which contain both bound and unbound dyes. The green circle symbols are related to the absorption intensities of the supernatant solutions that contain the unbound dyes. The red dashed curves are obtained by subtraction of the green from the blue values and show the absorption caused by the bound dyes.

on the surface of the UCNCs. Such a strong dye–UCNC attachment and hence a shorter distance between the dye and Ln^{3+} are expected to be favorable for efficient energy transfer.[28,36]

(ii) Cy 740 and Cy 784 dyes do not bear carboxylic groups and can attach to the surface of UCNCs through coordination with sulfo groups. As can be seen in Fig. 2C and D, the absorbance of both dye-sensitized UCNC and supernatant solutions decreases continuously after each purification step. Since the absorbance of supernatant solutions approaches zero only after five purification steps, this indicates that the attached and free dyes are in dynamic equilibrium, so some dyes can detach from the surface of the UCNCs via rinsing with fresh MeOH. However, these results also suggest that after five purification steps, ∼20 molecules of Cy 740 and ∼14 molecules of the Cy 784 dye are adsorbed by each UCNC.

(iii) In contrast to the previous dyes, the Cy 748 dye also contains the carboxylic acid functional groups, while the sulfonate tail group has been replaced with an iodide counter ion. This molecule (as well as Cy 778 with a methoxycarbonyl group) interacts weakly with the surface of the particles, with all dye molecules being washed out during the first purification steps and transferred to the supernatant. Due to the lack of bound dyes, such UCNCs display no dye absorption (Fig. 2E and F). Hydrophilic NaGdF$_4$ and NaYF$_4$ nanocrystals have been

16316 | J. Mater. Chem. C, 2021, **9**, 16313–16323

This journal is © The Royal Society of Chemistry 2021

demonstrated by several authors to exhibit a positive zeta potential after the removal of OA.[44–46] Therefore, positively charged dyes do not have a high affinity to bind to the Ln^{3+} cations on the surface of UCNCs due to electrostatic repulsion.

In the discussion above, it was mentioned that the cyanine dyes can interact with the surface of $NaGdF_4$:Yb^{3+},Er^{3+} UCNCs via three well-distinguished mechanisms, as summarized in Fig. 3A. In this regard, FTIR spectra of the dye-capped materials provide additional information to understand the surface chemistry of the modified UCNCs (Fig. S6 and S13, ESI†). FTIR results clearly show the presence of hydroxyl groups on the surface of all the synthesized UCNCs. Such hydroxyl groups originate from the HCl treatment process when all the oleate ligands are removed from the surface of the UCNCs.[41] In other words, the HCl treatment probably replaces all Ln^{3+}–oleate bonds with Ln^{3+}–OH bonds. Although the next step is the substitution of all –OH centers with the dye molecules, such a desirable ligand exchange process does not occur completely during the dye-sensitization process. Compared with –OH and oleate ligands, the cyanine dye molecules have a larger cross-sectional (footprint) area and exhibit an overall negative charge due to their sulfo groups. Therefore, both steric and electrostatic repulsive forces prevent the dense packing of dye molecules on the UCNC surface. For this reason, only a fraction of the surface Ln^{3+} ions can be sensitized by the dye molecules, so the maximum number of dye molecules at the surface of each UCNC (the dye : UCNC ratio) will be proportional to the ratio of the UCNC surface area to the effective physical area (surface coverage) of the dye molecules. These numbers can also be confirmed based on the experimental dye : UCNCs ratios reported in the literature. For example, the dye : UCNCs ratios for IR806-sensitized UCNCs of 12, 16, and 54 nm in size were reported to be 40, 73, and 830, respectively,[9,12,35] while the average surface area occupied by each IR806 molecule is around 11 nm^2. In the case of our ultrasmall $NaGdF_4$:Yb^{3+},Er^{3+} UCNCs with an average diameter of 6.5 nm (133 nm^2 surface area), only $\sim$14–20 dye molecules can be placed on the surface of each particle, giving the average surface area occupied by

each dye molecule as $\sim$7–10 nm^2. In turn, we estimated the projected molecular areas of Cy 748 and Cy 792 from the geometries optimized at the B3LYP/6-31G(d,p) level to be 1.7 and 2.5 nm^2, respectively, when lying flat on the surface, and 1.1 and 2.4 nm^2 when perpendicular to the surface. This indicates that many –OH groups might remain on the surface of dye-sensitized UCNCs and are attached to the half-coordinated surface lanthanide ions to maintain the charge neutrality.[47] Meanwhile, such surface-anchored –OH groups have been demonstrated to be very efficient quenchers of the excited states of Yb^{3+} and Er^{3+} ions.[48–50]

Dye sensitization of $NaGdF_4$:Yb^{3+},Er^{3+} UCNCs

Cyanine dyes with broad absorption bands and high absorption cross-sections are strong photon absorbers; thus their efficient attachment on the surface of UCNCs is expected to result in an enhanced UC luminescence intensity. Here and below, the brightness parameter is used to discuss the intensity of the UC PL peaks assuming that the intensity is $\propto B_{UC}$. The UC luminescence spectra of Fig. 3B confirm that the dye-sensitization process strongly increases the luminescence of the UCNCs. The B_{UC} value for Cy 740-, Cy 754-, Cy 784-, and Cy 792-sensitized UCNCs – when excited at 740, 754, 784, and 792 nm, respectively – is 23-, 47-, 5-, and 65-fold higher than that of OA-capped UCNCs excited at 980 nm (at similar excitation intensities of 75 W cm^{-2} for all excitation wavelengths). The emission spectra of the dye-sensitized UCNCs consist of the green emission of Er^{3+} exhibiting maxima at 520 and 540 nm ($^2H_{11/2} \rightarrow {}^4I_{15/2}$ and $^4S_{3/2} \rightarrow {}^4I_{15/2}$ transitions, respectively) and the red emission at 654 nm ($^4F_{9/2} \rightarrow {}^4I_{15/2}$ transitions). However, the red emission of UCNCs is highly reabsorbed by the dye molecules, since the cyanine dyes have a relatively high absorption around 654 nm (Fig. 1D). The emission shoulder at wavelengths of $>$600 nm can be attributed to anti-Stokes dye emissions, those that were not absorbed by UCNCs or transferred from the Er^{3+} ion back to the dye for re-emission. Such anti-Stokes dye emissions are not observed under excitation using 748 and 778 nm lasers if the dyes are removed by purification

Fig. 3 (A) Schematic of cyanine dye attachment mechanisms at the surface of $NaGdF_4$:Yb,Er UCNCs. (B) Upconversion emission spectra of different dye-sensitized UCNCs in MeOH, and OA-capped UCNCs in toluene. All measurements for dye-sensitized UCNCs were performed in MeOH solutions, under air, and after two purification processes (see Section 7 for detailed information, ESI†). Cy 740-, Cy 748-, Cy 754-, Cy 778-, Cy 784-, Cy 792-sensitized and OA-capped UCNCs were excited using 740, 748, 754, 778, 784, 792, and 980 nm laser lines, respectively (excitation intensity of 75 W cm^{-2} in all the experiments). (C) Absorption spectra of dye-sensitized UCNCs in MeOH.

(designated as Cy 748 and Cy 778 in Fig. 3B), which proves the origin of the luminescence signal (>600 nm). In addition, detection of the anti-Stokes dye emission also indicates a very low ϕ_{UC} of 6.5 nm UCNCs.

According to Fig. 3B, the different B_{UC} values of the dye-sensitized UCNCs can be clarified according to the three above-mentioned types of dye–UCNC interaction. As expected, sensitization with Cy 748 and Cy 778 dyes does not enhance the UC luminescence, since no organic dyes are attached to the surface of the UCNCs. By contrast, strong bonding of the Cy 754 and Cy 792 dyes results in the highest B_{UC} enhancement. Finally, weaker bonding and greater distances between the Cy 740 and Cy 784 dye molecules and the surface of the UCNCs result in a lower UC luminescence intensity than that of Cy 754- and Cy 792-sensitized UCNCs.

Another factor that may affect the UC luminescence enhancement of different dye-sensitized UCNCs is the spectral match between the emission spectra of the dye molecules and the Yb^{3+} absorption at 980 nm. Good spectral overlap results in a more efficient energy transfer between the donating excited singlet state of the dyes and the $^2F_{5/2}$ accepting energy level of Yb^{3+}. Therefore, the higher B_{UC} of Cy 792-sensitized UCNCs can be explained by the better match between the luminescence of Cy 792 (Fig. 1E) and the absorption spectrum of Yb^{3+}. On the other hand, the spectral match for Cy-784 is better than that for Cy 754, but the latter enhances the B_{UC} value more. Thus, it is

assumed that stronger bonding (and so a shorter distance) between the dye and UCNC dominates over the better spectral overlap. Thus, Cy 792 and Cy 754 dyes demonstrate a stronger enhancement despite exhibiting a weaker absorption (Fig. 3C).

It is worth noting that increasing the dye concentration (to increase the number of adsorbed dyes) in the mixture with UCNCs has a negative effect on the B_{UC} enhancement. As indicated in Fig. S14 (ESI†), the luminescence intensity of different dye-sensitized UCNCs increases with an increasing dye concentration until a certain maximum value is achieved. After that, increasing the dye concentration resulted in a reduced B_{UC} value, because the excess free dyes do not transfer energy to the Yb^{3+} ions but instead reabsorb both the red and green UC radiation.

Effect of dye triplet states

Regarding the weak spectral match between the dye fluorescence and absorption band of the sensitizer ion (in this case, 980 nm for Yb^{3+}), energy transfer through the dye triplet states has been suggested for explaining the UC enhancement using dye sensitization.[35] To investigate the possibility of energy transfer through the dye triplet states, NaGdF$_4$:Yb^{3+},Er^{3+} UCNCs are mixed with different dyes in deuterated methanol (CD$_3$OD) under argon (Ar) and air. Dispersing the UCNCs in CD$_3$OD under oxygen-free conditions can reduce the amount of oxygen-induced quenching and increases the triplet-state lifetime.

Fig. 4 (A) Upconversion emission spectra of different dye-sensitized UCNCs in CD$_3$OD and OA-capped UCNCs in toluene. The conjugation with dyes was done under Ar, using the optimum dye : UCNCs ratios, and without further purification processes. Cy 740-, Cy 754-, Cy 784-, and Cy 792-sensitized, and OA-capped UCNCs were excited with 740, 754, 784, 792, and 980 nm lasers, respectively (excitation power of 75 W cm^{-2}). (B) Proposed energy-level diagram and sequential energy-transfer paths of dye-sensitized NaGdF$_4$:Yb,Er UCNCs. (C)–(F) Comparing the UC luminescence for solutions of Cy 740-, Cy 754-, Cy 784-, and Cy 792-sensitized UCNCs prepared under Ar and air. The legend (1 h air) corresponds to the UC luminescence of solutions prepared under Ar and exposed to air for 1 hour. All the solutions have the same UCNCs concentrations, prepared using the optimum dye : UCNCs ratios, without further purification processes. The UCNCs prepared in air and Ar were dispersed in MeOH and CD$_3$OD, respectively.

16318 | *J. Mater. Chem. C*, 2021, **9**, 16313–16323

This journal is © The Royal Society of Chemistry 2021

Thus, an increase in UC intensity in the absence of oxygen may indicate the involvement of triplet states in the sensitization process. Indeed, significant UC enhancement was observed in the quencher-free medium (Fig. 4A). Note that the same concentrations of dye and UCNCs were used for sensitizing the UCNCs in both Ar and air media (the corresponding absorption spectra are given in Fig. S15 and S16, ESI†). In the case of dye sensitization in a quencher-free medium, the B_{UC} values for the Cy 740-, Cy 754-, Cy 784-, and Cy 792-sensitized UCNCs were, respectively, ~ 40, ~ 255, ~ 2, and ~ 220 times higher than that of OA-capped UCNCs. Moreover, such B_{UC} enhancement is greater than those previously measured for the same UCNCs sensitized in MeOH and an air environment (up to ~ 23-, ~ 47-, and ~ 65-times UC luminescence enhancement for Cy 740-, Cy 754-, and Cy 792-sensitized UCNCs, respectively).

Accordingly, the energy-transfer mechanism between the cyanine dyes and the UCNCs can be depicted by the schematic of Fig. 4B. When the dyes are excited, they first go to singlet (S_1) excited states. The energy transfer from the dye to the Yb^{3+} ions of the UCNCs can be realized via two paths: (i) Förster- or Dexter-type energy transfer (ET) from the singlet state; and/or (ii) a two-step energy transfer including ISC within the dye from the singlet excited state to the triplet (T_1) excited state and then energy transfer to the $^2F_{5/2}$ state of the Yb^{3+} ion via the Dexter mechanism. The latter process is significant only at very short donor–acceptor distances (~ 1 nm or less), while Förster energy transfer can occur over longer distances (1–10 nm).[3]

Interestingly, when the dye-sensitized UCNCs in CD_3OD were transferred from Ar to air via simply opening the cuvette (Fig. 4C and E), a very small change in B_{UC} was observed for UCNCs sensitized with Cy 740 and Cy 784 dyes. The observed effect is consistent with the earlier assumption of a longer distance between these dyes and the UCNCs, and thus triplet transfer can be ruled out for these dyes (as it is a short-distance process by the Dexter mechanism). In contrast, the B_{UC} of Cy 754- and Cy 792-sensitized UCNCs is drastically reduced upon opening the cuvettes (Fig. 4D and F). Likewise, the difference in B_{UC} observed for MeOH and CD_3OD solutions under an air atmosphere signifies the contribution of –OH groups to UC quenching. Thus, this simple experiment makes it possible to distinguish between the B_{UC} enhancement obtained by reducing the surface quenching induced by the –OH groups and reducing the triplet-state quenching.

In the literature, Garfield et al. reported energy transfer from the triplet states of the IR806 dye to $NaY(Gd)F_4$:Yb^{3+},Er^{3+} UCNCs as being effective for UC enhancement.[35] However, energy transfer in some other dye-sensitized UCNCs, like FITC-sensitized CaF_2: Nd^{3+},Er^{3+},Yb^{3+} UCNCs, was realized exclusively via the excited singlet states without any evidence of activating the excited triplet states.[28] Thus, it seems that several factors affect the competition between the direct ET and the two-step (ISC + ET) energy-transfer pathways in the dye-sensitized UCNCs. In this work, sensitization with Cy 754 and Cy 792 dyes leads to the more efficient ET from the dyes' triplet state to the UCNCs and subsequently a stronger B_{UC} enhancement. Moreover, the assumption that the Cy 740 dye

can exhibit a high level of sensitization through the triplet state due to the heavy-atom effect of iodine[37] and thus enhancing ISC is proved to be incorrect. Instead, it appears that shorter dye–NC distances (i.e., stronger binding) are crucially important for triplet–Ln^{3+} energy transfer.

Furthermore, the synthesis of $NaY_{0.50}Gd_{0.30}F_4$:$Yb_{0.18}$,$Er_{0.02}$ UCNCs with an optimized concentration of heavy lanthanide ions (Fig. S17 and S18, ESI†) and sensitizing the UCNCs with the cyanine dyes resulted in a significant UC luminescence enhancement with respect to that of the dye-sensitized $NaGd_{0.80}F_4$:Yb^{3+},Er^{3+} UCNCs (Fig. S19 and S20, ESI†). However, these UCNCs exhibit a large size and an elliptical shape (18.2 × 23.8 nm) and cannot be directly compared with $NaGdF_4$:Yb^{3+},Er^{3+} UCNCs. Further discussion on the effect of the composition of UCNCs and B_{UC} enhancement is presented in Section 9 (ESI†).

Dye sensitization of core@shell UCNCs

Although the core@shell UCNCs are known to prevent surface quenching of the luminescence and lead to higher B_{UC} and ϕ_{UC}, designing an appropriate shell layer that results in an efficient ET from the dye to the core UCNCs is somewhat challenging.[3,29] In the case of an inert (undoped) shell, the shell layer should be as thin as possible so as not to reduce the energy-transfer pathways from the dye to the active ions of the core.[28] While the thick inert shell reduces both Dexter- and Förster-based ET, a thin active shell strategy of co-doping with Yb^{3+} and Nd^{3+} is recognized as an effective tool for enhancing dye-sensitized UC.[29,34]

Here we investigate how the formation of shell layers with desired energy levels, relative to the energy levels of dye singlet/triplet states and Ln^{3+} energy levels in the core, can affect the efficient energy transfer from the dye to the core, and lead to further improvement of the B_{UC} in UCNCs. For this purpose, as-synthesized $NaGdF_4$:Yb^{3+},Er^{3+} UCNCs were coated with thin active $NaGdF_4$ shells with three lanthanide doping compositions: (i) 10% Yb^{3+}; (ii) 30% Nd^{3+}; and (iii) 10% Yb^{3+} and 30% Nd^{3+}. The dopant concentrations were chosen according to the optimized values reported in the literature.[9,23] Fig. 5A1–A3 show the high-angle annular dark-field scanning transmission electron microscopy (HAADF-STEM) micrographs and size-distribution histograms of the synthesized core@shell UCNCs. As can be seen, the synthesized UCNCs are highly monodisperse and their average size is around 10–11 nm, indicating that a shell thickness of ~ 2 nm had been grown onto the core UCNCs. The XRD patterns of Fig. S21 (ESI†) also confirm that the shell layers have a hexagonal β-phase crystal structure, similar to that of the core UCNCs.

All the synthesized UCNCs were coupled with Cy 740, Cy 754, Cy 784, and Cy 792 dyes in CD_3OD and under Ar. As can be seen in Fig. S22–S24 (ESI†), different core@shell UCNCs capped with the same dye exhibit almost the same absorption intensity, which is expected due to the identical size of the different UCNCs and therefore the same dye:UCNC ratio. Fig. 5B1 demonstrates that sensitizing the $NaGdF_4$:Yb^{3+},Er^{3+}@$NaGdF_4$: 10%Yb^{3+} UCNCs with Cy 740, Cy 754, Cy 784, and Cy 792 dyes

This journal is © The Royal Society of Chemistry 2021

J. Mater. Chem. C, 2021, 9, 16313–16323 | 16319

Fig. 5 (A1–A3) High-angle annular dark-field scanning transmission electron microscopy (HAADF-STEM) micrographs and size-distribution histograms, (B1–B3) UC luminescence spectra in CD_3OD, and (C1–C3), schematic of energy-transfer pathways of different types of dye-sensitized core@shell UCNCs (1, $NaGdF_4$:Yb,Er@$NaGdF_4$:10%Yb; 2, $NaGdF_4$:Yb,Er@$NaGdF_4$:30%Nd; and 3, $NaGdF_4$:Yb,Er@$NaGdF_4$:10%Yb,30%Nd). The dye-sensitization processes were performed under Ar, without further purification processes. Cy 740-, Cy 754-, Cy 784-, and Cy 792-sensitized, and OA-capped UCNCs were excited with 740, 754, 784, 792, and 980 nm lasers, respectively (excitation power of 75 W cm^{-2}).

leads to, respectively, 183-, 445-, 53-, and 331-fold B_{UC} enhancement, compared with OA-capped $NaGdF_4$:Yb^{3+},Er^{3+} UCNCs (and to, respectively, 115-, 280-, 33-, and 209-fold B_{UC} enhancement, compared with OA-capped $NaGdF_4$:Yb^{3+},Er^{3+}@ $NaGdF_4$:10%Yb^{3+} UCNCs). Such amounts of UC luminescence enhancements can be explained by three reasons: (i) the shell reduces (but not fully prevents) Er^{3+} luminescence quenching by the –OH groups on the surface of the UCNCs; (ii) the thin shells do not limit ET processes; and (iii) the same ET mechanism is realized for both dye-sensitized core-only and core@shell UCNCs if there are similar energy levels of the sensitizing ions (Yb^{3+}) in the shell and core (Fig. 5C1). In the last case, ET happens from both the singlet and triplet states of the dyes to the Yb^{3+} ions in the shell layer.

The Nd^{3+}-doped shell layers also enhance the B_{UC} of UCNCs (Fig. 5B2) to a level similar to the intensity of $NaGdF_4$: Yb^{3+},Er^{3+}@$NaGdF_4$:10%Yb^{3+} UCNCs. As indicated in Fig. S25 (ESI†), doping the Nd^{3+} ions into the shell layer causes a strong absorption of core@shell UCNCs around 800 nm. This

absorption band is highly consistent with the PL emission spectra of the investigated dyes, so a much more efficient ET is expected from the singlet state of the dyes to the Nd^{3+} ions in the shell. Here, the energy transfer from the triplet states of the dyes to the UCNCs seems to be limited, probably due to the higher energy state of the Nd^{3+}-doped shell layer with respect to the energy levels of dyes and Yb^{3+} sensitizers in the core. Therefore, the restriction of such an energy-transfer pathway might limit the B_{UC} enhancement in the case of Cy 740- and Cy 754-sensitized $NaGdF_4$:Yb^{3+},Er^{3+}@$NaGdF_4$:30%Nd^{3+} UCNCs (Fig. 5C2).

Moreover, one can expect back-energy transfer from the Er^{3+} emissive states to Nd^{3+}, at different exciton wavelengths of 740–792 nm, which might also reduce the UC intensity. In general, no clear advantage was observed in the case of Nd^{3+} doping the active shell compared with Yb^{3+} doping.

Interestingly, doping the shell layer with both Yb^{3+} and Nd^{3+} sensitizer ions results in the greatest UC enhancement of the dye-sensitized UCNCs. Compared with the OA-capped $NaGdF_4$:Yb^{3+},Er^{3+}

16320 | J. Mater. Chem. C, 2021, 9, 16313–16323

This journal is © The Royal Society of Chemistry 2021

UCNCs, the emission intensity of Cy 740-, Cy 754-, Cy 784-, and Cy 792-sensitized $NaGdF_4:Yb^{3+},Er^{3+}@NaGdF_4:10\%Yb^{3+},30\%Nd^{3+}$ UCNCs was increased up to 236-, 680-, 75-, and 612-times, respectively (Fig. 5B3). As schematically shown in Fig. 5C3, doping both the Yb^{3+} and Nd^{3+} ions in the shell leads to the construction of dye-sensitized UCNCs that afford cascade energy transfer. The dye molecules on the surface of the core@shell UCNCs absorb photons and transfer the excited energy to the Nd^{3+} and Yb^{3+} ions of the shell. Although energy transfer is limited from the T_1 levels to the Nd^{3+} ions, energy transfer from the T_1 states to the Yb^{3+} ions of the shells leads to efficient energy conduction from the dye to the shell layer. This is followed by ET from the Nd^{3+} and Yb^{3+} ions of the shell layer to the Yb^{3+} ions of the core. Subsequently, intra-core energy migration and energy transfer from Yb^{3+} to Er^{3+} ions result in the brightest UCNCs.

Absolute quantum yield of $NaGdF_4:Yb^{3+},Er^{3+}@NaGdF_4:30\%Nd^{3+}$ UCNCs

Although all dye-sensitized UCNCs demonstrate an enhanced B_{UC} compared with excitation of the same UCNCs using a 980 nm laser, the origin of the enhancement requires better understanding in order to further improve the properties of dye-sensitized UCNCs. Fig. 6 presents the intensity dependence of ϕ_{UC} for OA-capped and Cy 792-sensitized $NaGdF_4:Yb^{3+}$, $Er^{3+}@NaGdF_4:30\%Nd^{3+}$ UCNCs excited at 980 and 792 nm, respectively. The first important observation arising from these experimental results is that dye-sensitized UCNCs exhibit a ϕ_{UC} value that is approximately an order of magnitude lower than the same OA-capped UCNCs (before the ligand-exchange step) when excited with a 980 nm laser. As previously discussed, treatment with HCl results in a large number of –OH groups on the surface of the UCNCs. Most of such –OH groups remain on the surface after dye-sensitization and cause luminescence quenching. Although ϕ_{UC} decreases due to the quenching, the B_{UC} of the dye-sensitized UCNCs is higher than those of OA-capped ones

Fig. 6 Intensity dependence of the absolute UC quantum yield for $NaGdF_4$:Yb,Er@NaGdF$_4$:30%Nd UCNCs: OA–caped UCNCs before ligand exchange dispersed in toluene (black squares); UCNCs after ligand exchange with Cy 792 dye in CD$_3$OD under argon and without the purification process excited using a 980 nm (red circles) and a 792 nm (blue triangles) laser.

(Fig. 5B2). This phenomenon is explained by the very efficient collection of excitation energy by the dye antennas. While the ϕ_{UC} of dye-sensitized UCNCs decreases, the absorption enhancement dominates over the OH-group quenching, resulting in brighter UC luminescence. It can be assumed that the substitution of oleate by small nitrosonium tetrafluoroborate ($NOBF_4$) ligands is a good alternative to prevent OH^- formation on the surface of the UCNCs before the dye-sensitization process.[51]

The second important observation is that the ϕ_{UC} of Cy 792-sensitized UCNCs is constant, starting from the lowest excitation intensity of 3 W cm^{-2}. In general, two UC luminescence regimes can be expected, corresponding to low and high excitation intensity. Under low excitation intensity, the concentration of the $\{Er^{3+}:^4I_{11/2}$ and $Yb^{3+}:^2F_{5/2}\}$ manifold and the $Er^{3+}:^4I_{13/2}$ state is low and, thus, energy transfer upconversion (ETU) occurs slowly (rate of ETU $\ll$ monomolecular decay rate, which includes radiative and non-radiative decay, quenching and cross-relaxation). As a result, the UC quantum yield increases with increasing excitation intensity. Under a high excitation intensity, the concentration of the $\{Er^{3+}:^4I_{11/2}$ and $Yb^{3+}:^2F^{5/2}\}$ manifold and the $Er^{3+}:^4I_{13/2}$ state is high and a main part of the excited states annihilates via ETU (rate of ETU $\gg$ monomolecular decay rate). Under such conditions the upward trend of the UC quantum yield is saturated. The critical power density (CPD) determines the boundary between the two regimes.[52] The rate of generation of excited states depends on three factors: the number of incident photons (the excitation intensity), the absorption cross-section and the concentration of the sensitizer. As the absorption cross-section of the dye is approximately 10^5-fold higher compared with Yb^{3+}, the same excitation intensity gives an approximately 10^5-fold higher concentration of the $\{Er^{3+}:^4I_{11/2}$ & $Yb^{3+}:^2F_{5/2}\}$ manifold (under a similar number of Yb^{3+} ions and dye molecules per UCNC, as well as efficient energy transfer from the dye to Yb^{3+}).[15] Thus, excitation with a 792 nm laser can be expected to saturate the UC quantum yield, while excitation with 980 nm exhibits a linear increase in the UC quantum yield for both OA-caped and dye-sensitized UCNCs (Fig. 6). In other words, sensitization with dyes at a relatively low excitation intensity creates a high enough concentration of intermediate Er^{3+} states ($Er^{3+}:^4I_{11/2}$ and $Er^{3+}:^4I_{13/2}$) that annihilate faster than monomolecular (including quasi-monomolecular) quenching can occur.

However, the overall ϕ_{UC} does not exceed the ϕ_{UC} value obtained at 980 nm excitation using an excitation intensity of 100 W cm^{-2}. As can also be seen from Fig. 6, the thin active shell does not fully protect the emissive Er^{3+} states ($Er^{3+}:^4S_{3/2}$ and $Er^{3+}:^4F_{9/2}$) from surface quenching, which becomes the key loss mechanism. To conclude, in order to further improve ϕ_{UC} and B_{UC}, a smart approach for preventing surface quenching – but still enabling efficient ET from the dye to the Ln^{3+} ions – must be found.
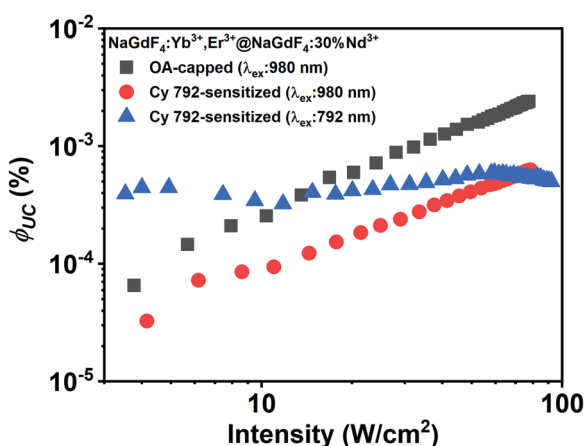
Conclusions

Cyanine dyes attach to the surface of ultrasmall $NaGdF_4$: Yb^{3+},Er^{3+} UCNCs ($\sim$6.5 nm) through chemical coordination

This journal is © The Royal Society of Chemistry 2021

J. Mater. Chem. C, 2021, **9**, 16313–16323 | **16321**

of the carboxylic acid group with Ln^{3+} ions (for Cy 754 and Cy 792 dyes) and electrostatic interaction between sulfonate groups and the surface of the UCNCs (for Cy 740 and Cy 784 dyes). By contrast, positively charged Cy 748 and Cy 778 dyes do not adsorb and do not play a sensitizing role. In the case of dye-sensitized UCNCs, the dye : UCNCs ratios were found to be ~ 14–20, depending on the size of the dye and the attachment mechanism. The attachment mechanism also determines the distance between the dyes and the UCNCs and, in turn, the involvement of dye triplet states in the sensitization of the UCNCs. Overall, the deprotection of OA-capped UCNCs using HCl leads to around a 10-times decrease in the UC quantum yield (measured in CD_3OD). If the dye-modified UCNCs are placed in methanol, a further strong decrease in UC luminescence is observed due to quenching induced by the hydroxyl group.

Despite the reduced UC quantum yield, the greatest UC luminescence enhancement (of 680- and 612-fold) was achieved with Cy 754 and Cy 792 dyes, respectively, adsorbed at $NaGdF_4$:Yb^{3+},Er^{3+}@$NaGdF_4$:10%Yb^{3+},30%Nd^{3+} UCNCs in deuterated methanol under oxygen-free conditions. The sensitization mechanism with the participation of dye triplet states was observed for these firmly bonded dyes. For dyes that interact more weakly (i.e., Cy 740 and Cy 784), an enhancement of the UC luminescence of 236- and 75-times, respectively, was measured. Modification of the chemical composition of the active shell ($NaGdF_4$:Yb^{3+},Er^{3+}@$NaGdF_4$:10%Yb^{3+} UCNCs were also investigated) leads to a slightly lower UC enhancement of 115-, 280-, 33-, and 209-fold for Cy 740, Cy 754, Cy 784, and Cy 792 dyes, respectively. A similar UC enhancement was also obtained for dye-sensitized $NaGdF_4$:Yb^{3+},Er^{3+}@$NaGdF_4$:30%Nd^{3+} UCNCs. It was suggested that co-doping with Yb^{3+} and Nd^{3+} ions in the shell layer facilitated a cascaded energy transfer from the dye singlet and triplet states to the Er^{3+} ions, while the shell singly-doped with Nd^{3+} or Yb^{3+} provides much less efficient energy transfer. In turn, UCNCs without the shell (but with the same core) demonstrate the weakest enhancement of 23-, 47-, 5-, and 65-fold for the Cy 740, Cy 754, Cy 784, and Cy 792 dyes, respectively.

Thus, we demonstrate that significant UC luminescence enhancement exists for dye-sensitized ultra-small core (6.5 nm)@shell (2 nm) UCNCs. To further enhance the brightness of the dye-sensitized UCNCs, surface quenching of the Er^{3+} luminescent states must be reduced, either by a novel ligand-exchange process or by clever design of the active shell.

Experimental

A detailed description of the chemicals, the synthesis of rare-earth acetate precursors, the synthesis of different cores and core@shell UCNCs, the synthesis of cyanine dyes and dye-sensitizing UCNCs, and the characterization methods (TGA, TEM, XRD, FTIR, absorption and photoluminescence emission) of the materials is given in the ESI.†

Author contributions

Conflicts of interest

There are no conflicts of interest to declare.

Acknowledgements

Notes and references

1 G. Chen, H. Qiu, P. N. Prasad and X. Chen, *Chem. Rev.*, 2014, **114**, 5161–5214.

2 D. Hudry, I. A. Howard, R. Popescu, D. Gerthsen and B. S. Richards, *Adv. Mater.*, 2019, **31**, 1900623.

3 X. Wang, R. R. Valiev, T. Y. Ohulchanskyy, H. Ågren, C. Yang and G. Chen, *Chem. Soc. Rev.*, 2017, **46**, 4150–4167.

4 G. Chen, H. Ågren, T. Y. Ohulchanskyy and P. N. Prasad, *Chem. Soc. Rev.*, 2015, **44**, 1680–1713.

5 Y. Liu, D. Tu, H. Zhu and X. Chen, *Chem. Soc. Rev.*, 2013, **42**, 6924–6958.

6 R. Weinstain, T. Slanina, D. Kand and P. Klán, *Chem. Rev.*, 2020, **120**, 13135–13272.

7 K.-L. Wong, J.-C. G. Bünzli and P. A. Tanner, *J. Lumin.*, 2020, **224**, 117256.

16322 | *J. Mater. Chem. C*, 2021, **9**, 16313–16323

This journal is © The Royal Society of Chemistry 2021

8 H. Dong, L.-D. Sun and C.-H. Yan, *Nanoscale*, 2013, **5**, 5703–5714.

9 G. Chen, J. Damasco, H. Qiu, W. Shao, T. Y. Ohulchanskyy, R. R. Valiev, X. Wu, G. Han, Y. Wang and C. Yang, *Nano Lett.*, 2015, **15**, 7400–7407.

10 L. Liang, X. Qin, K. Zheng and X. Liu, *Acc. Chem. Res.*, 2018, **52**, 228–236.

11 M. Saboktakin, X. Ye, U. K. Chettiar, N. Engheta, C. B. Murray and C. R. Kagan, *ACS Nano*, 2013, **7**, 7186–7192.

12 W. Zou, C. Visser, J. A. Maduro, M. S. Pshenichnikov and J. C. Hummelen, *Nat. Photonics*, 2012, **6**, 560–564.

13 D. Yin, Y. Liu, J. Tang, F. Zhao, Z. Chen, T. Zhang, X. Zhang, N. Chang, C. Wu and D. Chen, *Dalton Trans.*, 2016, **45**, 13392–13398.

14 C. G. Dupuy, T. L. Allen, G. M. Williams and D. Schut, *J. Nanotechnol.*, 2014, **2014**, 538163.

15 B. S. Richards, D. Hudry, D. Busko, A. Turshatov and I. A. Howard, *Chem. Rev.*, 2021, **121**, 9165–9195.

16 W. R. Algar, M. Massey, K. Rees, R. Higgins, K. D. Krause, G. H. Darwish, W. J. Peveler, Z. Xiao, H.-Y. Tsai, R. Gupta, K. Lix, M. V. Tran and H. Kim, *Chem. Rev.*, 2021, **121**, 9243–9358.

17 W. Ren, G. Lin, C. Clarke, J. Zhou and D. Jin, *Adv. Mater.*, 2020, **32**, 1901430.

18 X. Wu, H. Lee, O. Bilsel, Y. Zhang, Z. Li, T. Chen, Y. Liu, C. Duan, J. Shen and A. Punjabi, *Nanoscale*, 2015, **7**, 18424–18428.

19 M. Saleh, I. Panas, F. Frenzel, C. Würth, B. Rühle, Y. L. Slominskii, A. Demchenko and U. Resch-Genger, *Methods Appl. Fluoresc.*, 2019, **7**, 014003.

20 Y. Ji, F. Lu, Y. Tang, W. Qian, Q. Fan and W. Huang, *Inorg. Chem. Commun.*, 2020, **111**, 107640.

21 W. Wei, G. Chen, A. Baev, G. S. He, W. Shao, J. Damasco and P. N. Prasad, *J. Am. Chem. Soc.*, 2016, **138**, 15130–15133.

22 C. D. LaBoda and C. L. Dwyer, *Adv. Funct. Mater.*, 2016, **26**, 2866–2874.

23 X. Wu, Y. Zhang, K. Takle, O. Bilsel, Z. Li, H. Lee, Z. Zhang, D. Li, W. Fan and C. Duan, *ACS Nano*, 2016, **10**, 1060–1066.

24 R. Deng, J. Wang, R. Chen, W. Huang and X. Liu, *J. Am. Chem. Soc.*, 2016, **138**, 15972–15979.

25 C. Siefe, R. D. Mehlenbacher, C. S. Peng, Y. Zhang, S. Fischer, A. Lay, C. A. McLellan, A. P. Alivisatos, S. Chu and J. A. Dionne, *J. Am. Chem. Soc.*, 2019, **141**, 16997–17005.

26 Z. Wang and A. Meijerink, *J. Phys. Chem. Lett.*, 2018, **9**, 1522–1526.

27 D. Li, C. Li, X. Liu, Q. Cui, S. Xu and J. Qiu, *ChemNanoMat*, 2020, **6**, 285–291.

28 J. Liu, A. M. Kaczmarek, F. Artizzu and R. Van Deun, *ACS Photonics*, 2019, **6**, 659–666.

29 G. Chen, W. Shao, R. R. Valiev, T. Y. Ohulchanskyy, G. S. He, H. Ågren and P. N. Prasad, *Adv. Opt. Mater.*, 2016, **4**, 1760–1766.

30 S. Alyatkin, E. Ureña-Horno, B. Chen, O. L. Muskens, A. G. Kanaras and P. G. Lagoudakis, *J. Phys. Chem. C*, 2018, **122**, 18177–18184.

31 J. Ke, S. Lu, X. Shang, Y. Liu, H. Guo, W. You, X. Li, J. Xu, R. Li and Z. Chen, *Adv. Sci.*, 2019, **6**, 1901874.

32 F. Zhao, D. Yin, C. Wu, B. Liu, T. Chen, M. Guo, K. Huang, Z. Chen and Y. Zhang, *Dalton Trans.*, 2017, **46**, 16180–16189.

33 X. Zhang, W. Chen, X. Xie, Y. Li, D. Chen, Z. Chao, C. Liu, H. Ma, Y. Liu and H. Ju, *Angew. Chem., Int. Ed.*, 2019, **58**, 12117–12122.

34 Q. Shao, X. Li, P. Hua, G. Zhang, Y. Dong and J. Jiang, *J. Colloid Interface Sci.*, 2017, **486**, 121–127.

35 D. J. Garfield, N. J. Borys, S. M. Hamed, N. A. Torquato, C. A. Tajon, B. Tian, B. Shevitski, E. S. Barnard, Y. D. Suh and S. Aloni, *Nat. Photonics*, 2018, **12**, 402–407.

36 J. Liu, P. Geiregat, L. Pilia, R. Van Deun and F. Artizzu, *Adv. Opt. Mater.*, 2021, **9**, 2001678.

37 L. Štacková, E. Muchová, M. Russo, P. Slavíček, P. Štacko and P. Klán, *J. Org. Chem.*, 2020, **85**, 9776–9790.

38 F. Wang, R. Deng and X. Liu, *Nat. Protoc.*, 2014, **9**, 1634.

39 D. Hudry, D. Busko, R. Popescu, D. Gerthsen, A. M. Abeykoon, C. Kübel, T. Bergfeldt and B. S. Richards, *Chem. Mater.*, 2017, **29**, 9238–9246.

40 L. Štacková, P. Štacko and P. Klán, *J. Am. Chem. Soc.*, 2019, **141**, 7155–7162.

41 N. Bogdan, F. Vetrone, G. A. Ozin and J. A. Capobianco, *Nano Lett.*, 2011, **11**, 835–840.

42 W. Kong, T. Sun, B. Chen, X. Chen, F. Ai, X. Zhu, M. Li, W. Zhang, G. Zhu and F. Wang, *Inorg. Chem.*, 2017, **56**, 872–877.

43 N. Jurga, D. Przybylska, P. Kamiński, A. Tymiński, B. F. Grześkowiak and T. Grzyb, *J. Colloid Interface Sci.*, 2022, **606**, 1421–1434.

44 G. Chen, T. Y. Ohulchanskyy, S. Liu, W.-C. Law, F. Wu, M. T. Swihart, H. Ågren and P. N. Prasad, *ACS Nano*, 2012, **6**, 2969–2977.

45 U. Kostiv, H. Engstová, B. Krajnik, M. Šlouf, V. Proks, A. Podhorodecki, P. Ježek and D. Horák, *Front. Chem.*, 2020, **8**, 497.

46 R. Li, X. Fang, J. Ren, B. Chen, X. Yuan, X. Pan, P. Zhang, L. Zhang, D. Tu, Z. Fang, X. Chen and Q. Ju, *Nanoscale*, 2021, **13**, 12494–12504.

47 D. Zherebetskyy, M. Scheele, Y. Zhang, N. Bronstein, C. Thompson, D. Britt, M. Salmeron, P. Alivisatos and L.-W. Wang, *Science*, 2014, **344**, 1380–1384.

48 F. T. Rabouw, P. T. Prins, P. Villanueva-Delgado, M. Castelijns, R. G. Geitenbeek and A. Meijerink, *ACS Nano*, 2018, **12**, 4812–4823.

49 Y. Wang, L. Tu, J. Zhao, Y. Sun, X. Kong and H. Zhang, *J. Phys. Chem. C*, 2009, **113**, 7164–7169.

50 H. Zhu, X. Chen, L. M. Jin, Q. J. Wang, F. Wang and S. F. Yu, *ACS Nano*, 2013, **7**, 11420–11426.

51 W. Shao, G. Chen, A. Kuzmin, H. L. Kutscher, A. Pliss, T. Y. Ohulchanskyy and P. N. Prasad, *J. Am. Chem. Soc.*, 2016, **138**, 16192–16195.

52 R. E. Joseph, C. Jiménez, D. Hudry, G. Gao, D. Busko, D. Biner, A. Turshatov, K. Krämer, B. S. Richards and I. A. Howard, *J. Phys. Chem. A*, 2019, **123**, 6799–6811.

This journal is © The Royal Society of Chemistry 2021

J. Mater. Chem. C, 2021, **9**, 16313–16323 | **16323**